



**HAL**  
open science

## **Kondo scale and coupled fluorescence across the $\gamma$ - $\alpha$ transition in Ce 0.93 Sc 0.07**

Bodry Tegomo Chiogo, Alessandro Nicolaou, Thierry Schweitzer, T. Mazet, Ashish Chainani, Daniel Malterre

► **To cite this version:**

Bodry Tegomo Chiogo, Alessandro Nicolaou, Thierry Schweitzer, T. Mazet, Ashish Chainani, et al.. Kondo scale and coupled fluorescence across the  $\gamma$ - $\alpha$  transition in Ce 0.93 Sc 0.07. *Physical Review B*, 2023, 108 (19), pp.195110. 10.1103/PhysRevB.108.195110 . hal-04274280




**HAL Id: hal-04274280**

**<https://hal.science/hal-04274280>**

Submitted on 7 Nov 2023

**HAL** is a multi-disciplinary open access archive for the deposit and dissemination of scientific research documents, whether they are published or not. The documents may come from teaching and research institutions in France or abroad, or from public or private research centers.

L'archive ouverte pluridisciplinaire **HAL**, est destinée au dépôt et à la diffusion de documents scientifiques de niveau recherche, publiés ou non, émanant des établissements d'enseignement et de recherche français ou étrangers, des laboratoires publics ou privés.

**Kondo scale and coupled fluorescence across the  $\gamma$ - $\alpha$  transition in  $\text{Ce}_{0.93}\text{Sc}_{0.07}$** B. Tegomo Chiogo <sup>1,2,\*</sup>, A. Nicolaou,<sup>3</sup> T. Schweitzer,<sup>1</sup> T. Mazet <sup>1</sup>, A. Chainani <sup>4</sup>, and D. Malterre<sup>1</sup><sup>1</sup>Université de Lorraine, CNRS, Institut Jean Lamour, F-54000 Nancy, France<sup>2</sup>Helmholtz-Zentrum Berlin für Materialien und Energie, Hahn-Meitner-Platz 1, Berlin D-14109, Germany<sup>3</sup>Synchrotron SOLEIL, L'Orme des Merisiers, Saint-Aubin, Boîte Postale 48, F-91192 Gif-sur-Yvette, France<sup>4</sup>National Synchrotron Radiation Research Center, Hsinchu Science Park, Hsinchu 30076, Taiwan

(Received 16 July 2023; accepted 20 October 2023; published 7 November 2023)

We present a resonant inelastic x-ray scattering (RIXS) study across the temperature ( $T$ ) driven  $\gamma$ - $\alpha$  transition in  $\text{Ce}_{0.93}\text{Sc}_{0.07}$ . RIXS measurements across the Ce  $M_5$  edge unambiguously identify the  $f^1 \rightarrow f^0$  and  $f^1 \rightarrow f^2$  charge excitations, which provide a quantification of the Ce on-site Coulomb repulsion energy,  $U_{ff}$ . Calculation with a simplified single-impurity Anderson model combined with full multiplet theory reproduces the charge excitations and establishes that the very different Kondo temperatures of the  $\gamma$  to  $\alpha$  phase are reflected in RIXS spectra. A systematic  $T$ -dependent hysteresis is observed for the  $f^0$  final state spectral intensity upon cycling across the  $\gamma$ - $\alpha$  transition. In addition, a fluorescencelike structure also follows the same hysteretic behavior and shows it is directly connected to the weight of the  $f^0$  configuration in the ground state. The results indicate that the Ce  $M$ -edge RIXS is a reliable quantitative probe of the electronic structure of strongly correlated Ce-based Kondo systems and is sensitive to the emergent Kondo energy scale.

DOI: [10.1103/PhysRevB.108.195110](https://doi.org/10.1103/PhysRevB.108.195110)**I. INTRODUCTION**

Cerium compounds comprise a particularly interesting subgroup of rare-earth materials owing to their large variety of magnetic, electronic, and structural properties [1–3]. The first-order isostructural phase transition in cerium metal is particularly important as it represents a prototypical case for testing the evolution of the Kondo effect from a small Kondo temperature ( $T_K$ ) to a very large  $T_K$  in the same material. Cerium undergoes a transition from a  $\gamma$  phase (with a localized magnetic moment and a small  $T_K$ ) stable at ambient conditions, to an  $\alpha$  phase (with an intermediate valence and a very large  $T_K$ ) at low temperature or high pressure [4]. This transition is associated with a volume collapse of about 15% and a loss of magnetic moments [4]. The first-order isostructural  $\gamma$ - $\alpha$  phase transition in cerium has attracted considerable interest in the last 50 years, both experimentally and theoretically [5–19].

RIXS has emerged as the preferred technique of probing elementary excitations such as magnons, phonons,  $d$ - $d$  excitations, charge-transfer excitations, etc., in various systems [20,21]. It is a photon in-photon out bulk-sensitive technique (probing depth  $> 100$ 's nanometers), unlike strongly surface sensitive photoemission spectroscopy (PES) and inverse photoemission spectroscopy (IPES), which give rise to surface features that complicate analyses of intrinsic bulk-sensitive spectra [22–24]. RIXS is a valuable tool for direct characterization of Kondo materials, yielding access to charge [25–28], spin-orbit, and crystal-field excitations [29–34], as well as the Kondo resonance [35–37]. These local electronic excitations

appear at fixed (Raman-like) loss energies  $h\nu_{\text{loss}} = h\nu_{\text{in}} - h\nu_{\text{out}}$  while scanning incident photon energy  $h\nu_{\text{in}}$  across the x-ray absorption spectrum. RIXS spectra also exhibit loss energy features that linearly disperse (fluorescencelike) as a function of  $h\nu_{\text{in}}$ , reflecting the delocalized electronic excitations [28,38–40]. Fluorescencelike features have also been observed in RIXS spectra at the  $L$  edge of transition metal oxides [41–43] where it is used to address the localization of charge excitations and versus itinerancy of charge carriers [41,42]. Currently, the origin of fluorescencelike features is under strong debate in the literature. Bisogni *et al.* [44] observed a low energy fluorescencelike structure in the  $L$ -edge RIXS spectra of  $\text{NdNiO}_3$  compound and concluded that the gap opening at low temperature is related to the  $T$  dependence of the fluorescencelike structure. They proposed that the fluorescence feature reflects unbound particle-hole pairs in the final state of RIXS. However, Pfaff *et al.* [42] investigated localized and delocalized Ti  $3d$  carriers in  $\text{LaAlO}_3/\text{SrTiO}_3$  with RIXS and suggested that the fluorescencelike structure is related to intermediate states of RIXS. This has been theoretically supported by Hariki *et al.* [45] using a combination of local-density approximation with dynamical mean-field theory. Recently, we reported a RIXS study on the detailed electronic structure of a  $\gamma$ -like cerium compound  $\text{CeAgSb}_2$  [40]. The Ce  $M$ -edge RIXS showed two Raman-like features corresponding to  $f^0$  and  $f^2$  final states, the Kondo singlet ground state merging into a quasielastic peak, the excited manifold of magnetic  $f^1$  states and a fluorescencelike feature. A simplified single-impurity Anderson model calculation with full multiplets could account for all charge excitations except the fluorescencelike feature. However, the fluorescencelike feature exhibited a clear  $T$  dependence, and it was conjectured that it reflected the Kondo energy scale.

\*Corresponding author: [bodry.tegomo\\_chiogo@helmholtz-berlin.de](mailto:bodry.tegomo_chiogo@helmholtz-berlin.de)

Thus, RIXS of Ce compounds exhibits complex spectra, along with the presence of Raman-like and fluorescencelike structures. However, while several studies have addressed the crystal field and spin-orbit splitting in Ce compounds, very few measurements have addressed the Kondo effect in RIXS over large energy scales. In particular, to understand the systematics in electronic parameters spanning from low  $T_K$  to high  $T_K$  Ce compounds, the RIXS spectra of different compounds need to be compared. Thanks to the unique properties of Ce metal, these modifications can be obtained in the same compound as a function of  $T$ . In order to identify all the salient features in cerium RIXS spectra and gain further insight into the origin of the fluorescencelike features, we have investigated the electronic structure of the  $\text{Ce}_{0.93}\text{Sc}_{0.07}$  alloy using Ce  $M_5$ -edge RIXS. This system is well known to exhibit the  $\gamma$ - $\alpha$  first-order isostructural transition as a function of  $T$ . Several spectroscopic measurements have analyzed the driving mechanism of the isostructural  $\gamma$ - $\alpha$  phase transition in cerium [5–17]. State-of-the-art PES on cerium obtained by Weschke *et al.* [11] revealed a peak at  $\sim 2$  eV below the Fermi level ( $E_F$ ), and another peak in the vicinity of  $E_F$ . These two peaks are respectively associated with the  $f^0$  and  $f^1$  final states and reflect the delocalized and localized states of the Kondo singlet ground state. The clearest spectral fingerprint of the  $\gamma$ - $\alpha$  phase transition was revealed by IPES [18] and resonant IPES [19] in the form of a  $T$ -dependent Kondo resonance across the transition. The  $\gamma$ - $\alpha$  transition was also investigated by Ce- $L_3$ -edge RIXS of  $\text{Ce}_{0.93}\text{Sc}_{0.07}$  by Rueff *et al.* [5] by tracking the  $T$ -dependent  $f^1/f^2$  intensity ratio. Simultaneously, Dallera *et al.* [6] also evidenced the  $\gamma$ - $\alpha$  transition by following the  $f^1$  intensity of Ce- $M_{4,5}$  x-ray absorption spectra. They also performed RIXS measurements at the Ce- $M_5$ -edge [6] and identified the  $f^0$  and  $f^1$  final states, but the  $f^2$  final state feature was not identified by measurements done at  $h\nu_{\text{in}}$  of the XAS  $M_5$ -edge peak and the  $M_5$  satellite peak.

In this report, our Ce  $M_5$ -edge RIXS study of  $\text{Ce}_{0.93}\text{Sc}_{0.07}$  reveals well-defined features associated with the  $f^0$  and  $f^2$  final states, allowing us to determine the  $4f$  Coulomb interaction experimentally, defined as the energy of the process  $f^1 + f^1 \rightarrow f^0 + f^2$ . The  $T$  dependence of the  $f^0$  final state and the fluorescencelike structure exhibit clear systematic changes across the  $\gamma$ - $\alpha$  transition with a very similar large hysteresis in  $T$  cycling. The results confirm that the fluorescencelike structure probes the weight of the  $f^0$  configuration in the ground state and its  $T$  dependence reflects the Kondo energy scale.

## II. EXPERIMENTAL DETAILS

Using the AERHA (Adjustable Energy Resolution High Acceptance) spectrometer [46] with a scattering angle of  $85^\circ$  at the SEXTANTS beamline [47] of synchrotron SOLEIL, the RIXS measurements were performed on a polycrystalline  $\text{Ce}_{0.93}\text{Sc}_{0.07}$  sample. The overall energy resolution, estimated from the full width at half maximum of the elastic peak, was about 350 meV, which is a little bit larger than the  $4f_{5/2}$ - $4f_{7/2}$  spin-orbit energy ( $\Delta_{\text{so}} = 280$  meV). A polycrystalline sample of  $\text{Ce}_{0.93}\text{Sc}_{0.07}$  was prepared by melting high-purity elements in an induction furnace under purified argon atmosphere. The ingot was melted ten times to ensure homogeneity for a weight

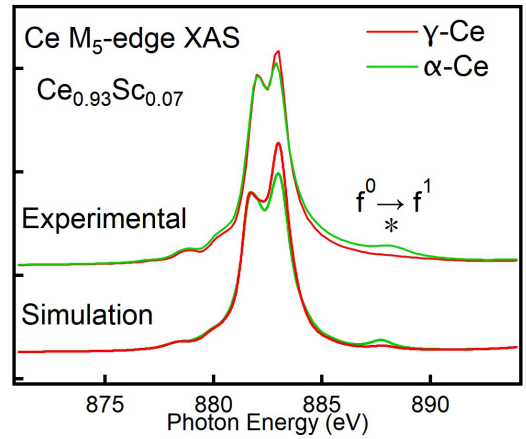


FIG. 1. Ce  $M_5$ -edge XAS spectra of  $\text{Ce}_{0.93}\text{Sc}_{0.07}$  measured at 20 K ( $\alpha$  phase) and 300 K ( $\gamma$  phase).

loss of  $\approx 0.5\%$ . The sample purity and crystal structure were verified by x-ray diffraction. Even though RIXS is bulk sensitive, the surface of the sample was cleaned *in situ* due to a surface oxidation feature seen in the total electron yield (TEY) Ce  $M$ -edge XAS spectrum. We found a weak but specific feature associated with oxidation in the TEY XAS spectrum, and its absence was used to ensure a clean surface (see Appendix A).

## III. RESULTS AND DISCUSSION

Figure 1 shows the Ce  $M_5$ -edge XAS spectra of  $\text{Ce}_{0.93}\text{Sc}_{0.07}$  measured at  $T = 20$  K ( $\alpha$  phase) and 300 K ( $\gamma$  phase). The Ce  $M_5$ -edge XAS is in good agreement with previously published data of  $\text{Ce}_{0.93}\text{Sc}_{0.07}$  [6]. The spectra are dominated by the  $3d^94f^2$  multiplets arising via the dipole transition from the  $4f^1$  contribution in the ground state but also have a finite contribution from the  $3d^94f^3$  multiplets coming from the  $4f^2$  contribution in the ground state (see Appendix B). The intermediate valence of the ground state is revealed via the  $3d^94f^1$  satellite at  $h\nu = 888$  eV. Its intensity reflects the weight of the  $f^0$  component in the ground state [48,49] and quantifies the amount of delocalization. In the  $\gamma$  phase, the XAS spectrum is consistent with an  $f$ -state occupation  $n_f \sim 1$  (very small satellite intensity), while in the  $\alpha$  phase, a significant increase of the intensity of the satellite is observed. Using a simplified single-impurity Anderson model with full multiplets, [40,50–52] using the Quany code [53,54] (see the Appendix B), we have simulated the spectra of the  $\gamma$  ( $\alpha$ ) phase corresponding to an intermediate valence ground state  $n_f = 0.982$  ( $n_f = 0.943$ ) which are consistent with the experimental spectra as shown in Fig. 1.

Figure 2 shows the Ce  $3d \rightarrow 4f \rightarrow 3d$  RIXS spectra of  $\text{Ce}_{0.93}\text{Sc}_{0.07}$  taken at (a)  $T = 20$  K ( $\alpha$  phase) and (b)  $T = 300$  K ( $\gamma$  phase) in  $\sigma$  and  $\pi$  polarizations, respectively. The spectra are shown as a function of the energy loss with the incident photon energy increasing in steps of 1 eV of the XAS spectrum, starting with  $M_5$  ( $h\nu = 883$  eV) up to  $M_5 + 7$  (2 eV above the  $f^1$  XAS satellite). In addition to the quasielastic  $f^1$  final state peak, the  $M_5$  and  $M_5 + 1$  spectra show clear  $f^2$  final state peaks in  $\sigma$  and  $\pi$  polarizations, while

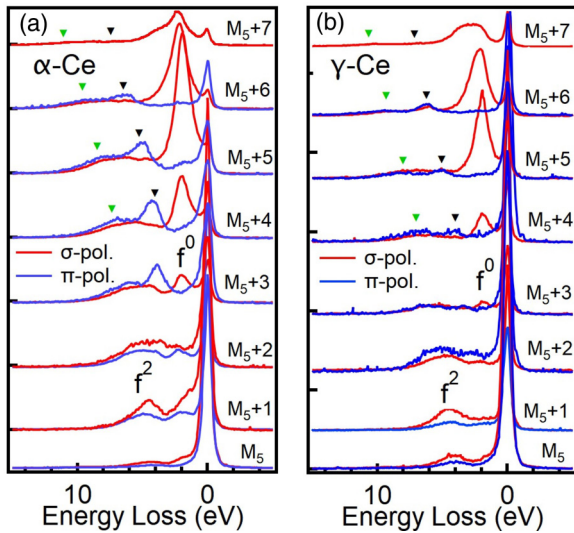


FIG. 2. Ce  $3d \rightarrow 4f \rightarrow 3d$  RIXS spectra of  $\text{Ce}_{0.93}\text{Sc}_{0.07}$  as a function of the energy loss. The measurements were performed at (a)  $T = 20$  K and (b)  $T = 300$  K for  $\sigma$  and  $\pi$  polarizations. The incident photon energy is tuned in steps of 1 eV of the XAS spectrum, starting with  $M_5$  up to  $M_5 + 7$  (2 eV above the  $f^1$  XAS satellite) (see Fig. 1).  $M_5$  denotes the excitation energy, which coincides with the maximum of the XAS spectrum ( $h\nu = 883$  eV). The green and black triangles indicate two different fluorescencelike features.

the spectra with incident energies  $M_5 + 5$  show the  $f^0$  final state peaks in  $\sigma$  polarization, consistent with our earlier study on  $\text{CeAgSb}_2$  [40]. It is noted that the  $f^2$  final states arise from the intermediate  $3d^9 4f^3$  XAS multiplet states, which in turn arise via the dipole transition from the  $4f^2$  component in the ground state [40]. The RIXS  $f^2$  final states show spectral shape changes as a function of incident energy. Further the  $f^2$  peak seen in the  $M_5$  and  $M_5 + 1$  spectra shows multiplet structure due to strong  $4f$ - $4f$  interactions, leading to the splitting of the  $f^2$  configuration into 13 multiplets according to the LS coupling,  $^3H$  ( $J = 4,5,6$ ),  $^3F$  ( $J = 2,3,4$ ),  $^1G$ ,  $^1D$ ,  $^3P$  ( $J = 0,1,2$ ),  $^1I$  and  $^1S$ . Indeed, when the incident photon energy is tuned at  $h\nu = M_5$ , the  $f^2$  final states are mainly the  $^3H$  multiplets. On increasing the incident photon energy from  $h\nu = M_5$  to  $h\nu = M_5 + 3$ , the  $f^2$  structure is composed of two main contributions whose spectral weight is photon dependent (see Appendix B). Similar multiplet effects have been observed for the  $f^2$  final state of RIPES at Ce  $N_{4,5}$  edge of cerium intermetallic compounds [55].

When the incident photon energy is tuned at the XAS satellite structure ( $M_5 + 5$ ), the RIXS spectra exhibit an intense peak at  $\sim 1.9$  eV with  $\sigma$  polarization, corresponding to the  $f^0$  final state in both  $\alpha$  phase and  $\gamma$  phase. In contrast to the  $f^2$  final state, this so-called  $f^0$  feature consists of a single peak with no multiplet effects. The  $^1S_0$  symmetry of the initial state in both phases is deduced from the drastic polarization dependence of the  $f^0$  final state, as was theoretically predicted [56,57] and experimentally observed [38,40]. By increasing the incident photon energy from  $M_5$  to  $M_5 + 7$ , the  $f^0$  structure is resonantly enhanced at  $M_5 + 5$  and remains at constant energy loss. On the other hand, the  $f^2$  final states show a Raman-type behavior with the incident photon energy

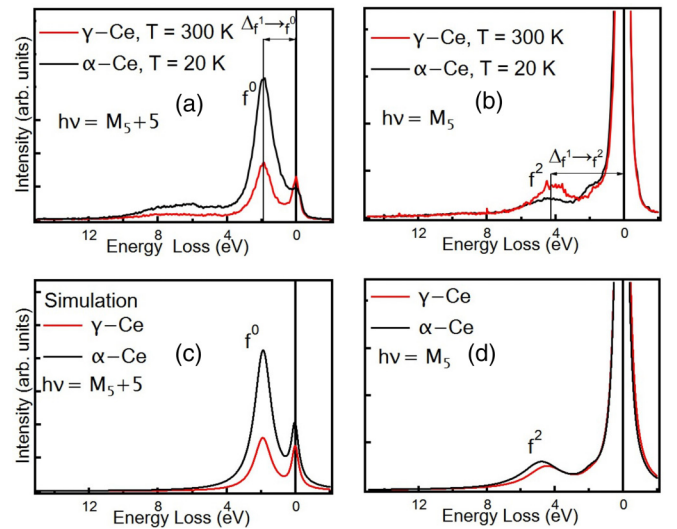


FIG. 3. Ce  $M_5$ -edge RIXS spectra of  $\text{Ce}_{0.93}\text{Sc}_{0.07}$  measured at 20 K ( $\alpha$  phase) and 300 K ( $\gamma$  phase) in  $\sigma$  polarization with the incident photon energy tuned at  $h\nu = M_5$  and  $h\nu = M_5 + 5$ . RIXS spectra of  $\alpha$  Ce and  $\gamma$  Ce calculated within the full-multiplet configuration interaction model in  $\sigma$  polarization at (a)  $h\nu = M_5 + 5$  and (b)  $h\nu = M_5$ . The parameters are given in Table I.

from  $M_5$  to  $M_5 + 3$ . In addition to this loss energy structures, the RIXS spectra from  $M_5 + 4$  to  $M_5 + 7$  also exhibit a fluorescencelike structure [see the black triangles in Figs. 2(a) and 2(b)]. The appearance of this structure in Figs. 2(a) and 2(b) is consistent with our previous study of the  $\text{CeAgSb}_2$  Kondo system. Interestingly, the RIXS spectra also exhibit another fluorescence feature indicated by the green triangles. The latter feature was not observed in our previous study in Ref. [40]. Surprisingly, the energy separation between these two fluorescence features corresponds to the energy separation between the  $f^0$  and  $f^2$  final states, which is about 2.7 eV. Therefore, the emission process of these fluorescence might be related to the continuum states through the  $f^0$  and  $f^2$  final states in the RIXS process. Moreover, we also found that their intensities in the  $\alpha$  phase are stronger compared to the  $\gamma$  phase. This indicates that the intensities of both structures are hybridization dependent and therefore related to the weight of the  $f^0$  configuration in the ground state. A tentative explanation of the fluorescencelike structure indicated by the black triangles was proposed to come from the electron-hole pair excitation related to the continuum [58,59]. However, more theoretical work is required to precisely understand what are the states involved in the initial, intermediate, and final state of the RIXS process giving rise to these fluorescence structures.

Figure 3(a) shows the comparison between the RIXS  $M_5 + 5$  spectra measured in the  $\alpha$ -phase and  $\gamma$ -phase with  $\sigma$  polarization to emphasize the  $T$ -dependence of the  $f^0$  peak. It is noteworthy that the spectral lineshape is unaffected by the transition. It is obvious that the  $f^0$  feature of  $\alpha$  Ce and  $\gamma$  Ce are located at the same energy  $\sim 1.9$  eV; however, the  $f^0$  feature of  $\alpha$  Ce is much more intense than that of  $\gamma$  Ce. This is consistent with the XAS spectra and indicates the very large  $T_K$  and strong delocalized character of  $4f$  states of  $\alpha$  Ce.



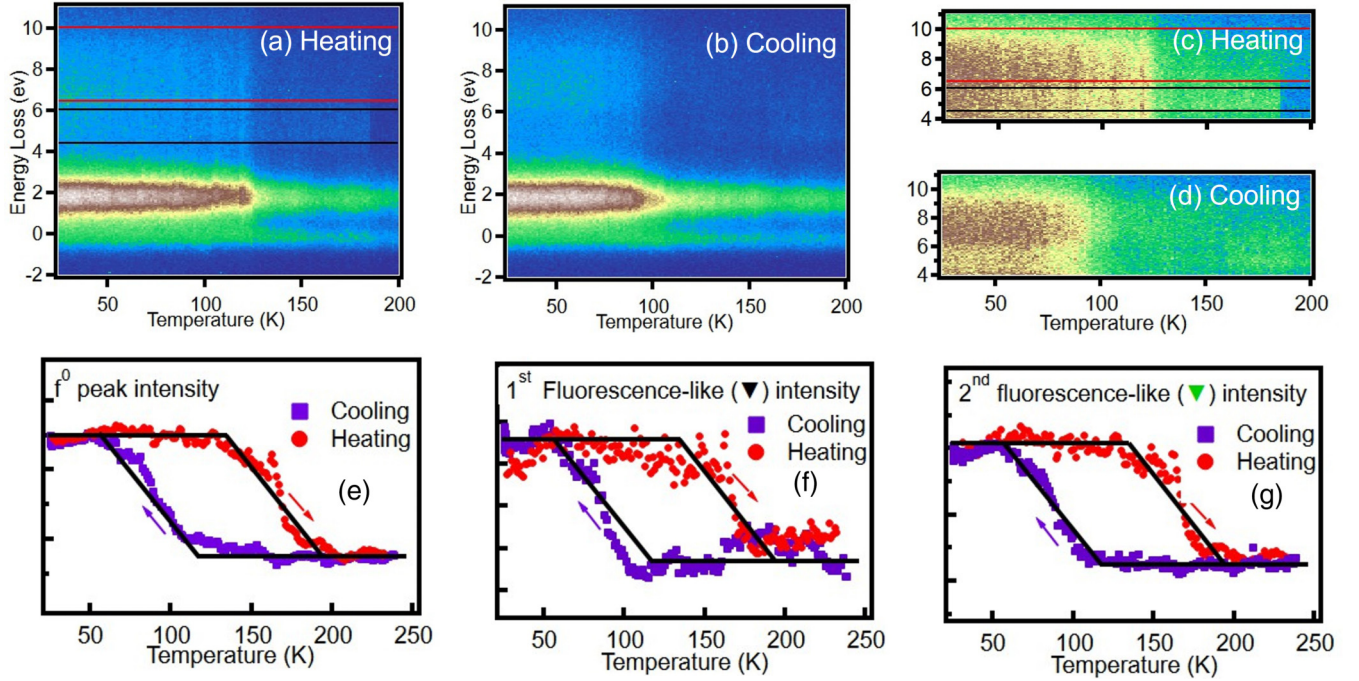


FIG. 4. (a)–(d) Highlighting of the  $\gamma$ - $\alpha$  transition with the  $T$ -dependent RIXS map measured in  $\sigma$  polarization with the incident photon energy  $h\nu = M_5 + 5$  [(c) and (d) are the RIXS map expanded in the region [of the fluorescence feature]]. Hysteresis loops derived from the integrated intensity of the (e)  $f^0$ , (f) first, and (g) second fluorescence-like structure (indicated by the black and green triangles in Fig. 2) in the RIXS map of  $\text{Ce}_{0.97}\text{Sc}_{0.07}$  [see Figs. 4(a) and 4(b)]. The arrows indicate the circulation inside the loop.

Similarly, the RIXS  $M_5$  spectra measured in the  $\alpha$  phase and  $\gamma$  phase with  $\sigma$  polarization to emphasize the  $T$  dependence of the  $f^2$  peak, which gets strongly reduced upon cooling [see Fig. 4(b)], consistent with  $L_3$ -edge RIXS measurements [5]. It should also be noted that the energy location of the  $f^0$  and  $f^2$  final states are consistent with PES and IPES results [19]. However, the intensity of the  $f^2$  feature is as strong as the intensity of the  $f^0$  final state in RIXS. Conversely, the intensity of the  $f^0$  feature in PES appears weak, like the  $f^2$  final state in RIXS. This is attributed to differences in cross sections for the different spectroscopic techniques, while the observed behavior in RIXS experiments is correctly obtained in our calculations. Figures 3(c) and 3(d) show the result of the simplified full-multiplet configuration interaction calculation of the RIXS spectra of  $\alpha$  Ce and  $\gamma$  Ce with the incident photon energy tuned at  $h\nu = M_5 + 5$  and  $h\nu = M_5$ , respectively (it should be noted that the calculations are performed at  $T = 0$ ). The parameters used for  $\alpha$  Ce and  $\gamma$  Ce are the same as given in Table I for  $T = 20$  K and 300 K spectra. The RIXS calculations are in satisfactory agreement with the experimental data in Fig. 3 except the position of the  $f^2$  structure in the

alpha phase, which is slightly overestimated. The presence of both  $f^0$  and  $f^2$  final states, respectively, at loss energy  $\Delta_{f^1 \rightarrow f^0}$  and  $\Delta_{f^1 \rightarrow f^2}$  allows us to directly determine the Coulomb repulsion  $U_{ff}$  in the  $\gamma$  and  $\alpha$  phases of  $\text{Ce}_{0.93}\text{Sc}_{0.07}$ . This is usually obtained by combining PES and IPES spectra [60,61]. The Coulomb repulsion  $U_{ff}$ , associated with removing a  $4f$  electron from one  $f$  site  $i$  and adding it to another  $f$  site  $j$ , is given by  $U_{ff} = \Delta_{f^1 \rightarrow f^0} + \Delta_{f^1 \rightarrow f^2}$ . The  $f^0$  and  $f^2$  structures are, respectively, located at about  $1.9 \text{ eV} \pm 0.1 \text{ eV}$  and  $4.5 \text{ eV} \pm 0.2 \text{ eV}$ , and accordingly, the Coulomb energy determined from RIXS is  $6.4 \text{ eV} \pm 0.3 \text{ eV}$ , consistent with the value of  $U_{ff}$  used for the XAS and RIXS calculations.

In order to investigate the spectral changes of the  $\gamma$ - $\alpha$  transition, we fixed the incident photon energy at the  $f^1$  XAS satellite ( $M_5 + 5$ , so as to maximize the RIXS  $f^0$  intensity) and then followed the evolution of the RIXS spectra over a complete cycle, from 20 K  $\rightarrow$  300 K  $\rightarrow$  20 K and the acquisition time of each RIXS spectrum was set to 40 seconds. The cooling and heating rate was 2 K/min. In the obtained RIXS color maps shown in Fig. 4(a) for the heating half-cycle and Fig. 4(b) for the cooling half-cycle, we observe clear

TABLE I.  $f^n$  contributions and  $f$ -state occupation ( $n_f$ ) for  $\gamma$  and  $\alpha$  Ce. Simplified SIAM parameters used for the calculations: the  $f$ - $f$  Coulomb exchange  $U_{ff}$ , the Coulomb interaction between  $f$  electron and  $3d$  core hole  $U_{fc}$ , the effective  $f$  binding energy  $\epsilon_f$ , and the hybridization strength  $V$  (all in eV).

|             | $f^0$ | $f^1$  | $f^2$  | $n_f$ | $\epsilon_f$ | $U_{ff}$ | $U_{fc}$ | $V$   |
|-------------|-------|--------|--------|-------|--------------|----------|----------|-------|
| $\alpha$ Ce | 7.46% | 90.79% | 1.747% | 0.943 | -1.35        | 6.38     | 9.93     | 0.148 |
| $\gamma$ Ce | 2.82% | 96.19% | 0.99%  | 0.982 | -1.57        | 6.38     | 9.93     | 0.105 |

changes in the region of the  $f^0$  charge excitations. Figure 4(e) shows the  $T$  dependence of the integrated intensities in the region of the  $f^0$  peak at 1.9 eV extracted from the RIXS maps. The onset of the phase transition is marked by a rapid decrease in the  $f^0$  intensity at 130 K on heating and a rapid increase at 110 K on cooling. A large hysteresis is observed, comparable to what is observed in the thermoelectric power and magnetization measurements [5,62]. Interestingly, the  $T$  dependence of the fluorescencelike structure [obtained from the same RIXS maps, see Fig. 4(f)] also exhibits a large hysteresis, similar to the one obtained from the intensity of the  $f^0$  structure. This confirms that the intensity of the fluorescencelike structure probes the weight of the  $f^0$  configuration in the initial ground state, and its  $T$  dependence reflects the change of the Kondo energy scale of  $\gamma$  Ce and  $\alpha$  Ce. Moreover, the temperature dependence of the  $f^2$  structure [see Fig. 4(g)] also exhibits a hysteresis confirming that change in the spectra due to the Kondo effect is also observed in the  $f^2$  structure as recently theoretically pointed out by N. Sasabe *et al.* [59]

#### IV. CONCLUSION

In conclusion, we investigated the  $T$ -dependence Ce- $M_5$  RIXS spectra of  $\text{Ce}_{0.93}\text{Sc}_{0.07}$  alloy across the isostructural  $\gamma$ - $\alpha$  phase transition. The results indicate RIXS is a valuable tool to obtain detailed information on the  $f$  electronic properties of Ce compounds in particular, and rare earths in general. We could deduce the electronic parameter evolution across the  $\gamma$ - $\alpha$  transition from the  $T$ -dependent spectra by tracking the spectral weight of the features corresponding to the  $f^1 \rightarrow f^0$  charge excitation. A systematic  $T$ -dependent hysteresis is observed for the  $f^0$  final state as well as the fluorescence structure spectral intensities upon cycling across the  $\gamma$ - $\alpha$  transition. The results establish a direct link between the fluorescencelike feature and the Kondo scale across the isostructural  $\gamma$ - $\alpha$  phase transition in  $\text{Ce}_{0.93}\text{Sc}_{0.07}$  alloy.

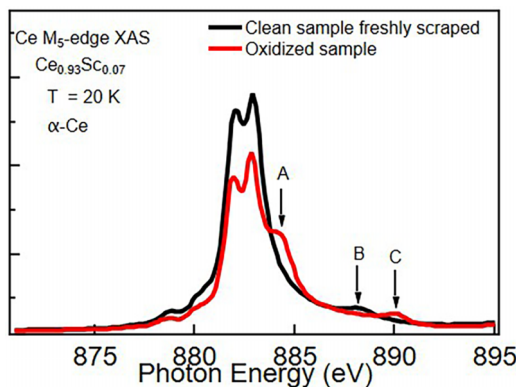


FIG. 5. Ce  $M_5$ -edge XAS spectra of  $\text{Ce}_{0.93}\text{Sc}_{0.07}$  at  $T = 20$  K with different surface qualities. The spectrum in the black line is taken from a freshly scraped sample, and the spectrum in the red line is taken from an oxidized surface. Arrows A and C indicate the contributions from oxidation effects of the aged surface.

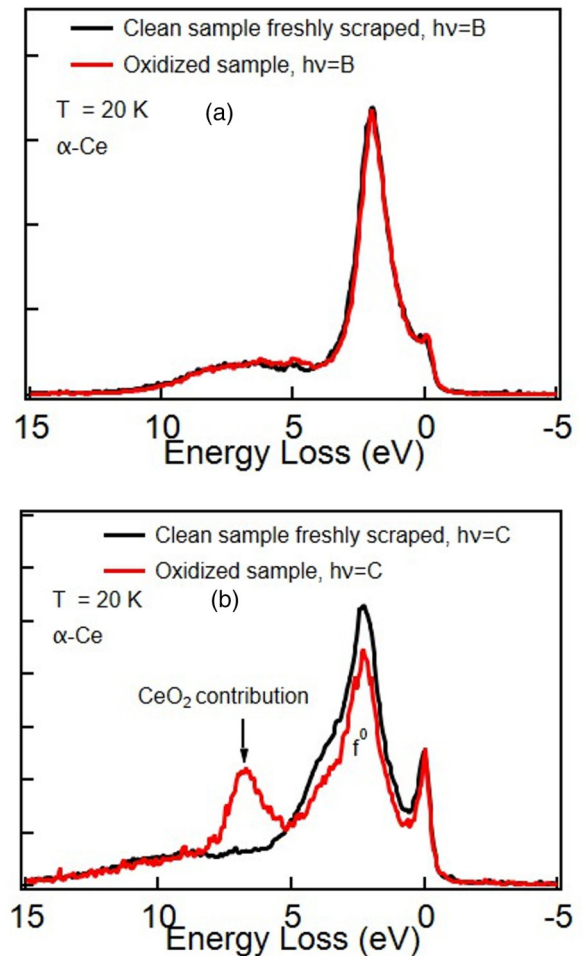


FIG. 6. Ce  $M_5$ -edge RIXS spectra taken at the incident photon energies (a)  $h\nu = B$  and (b)  $h\nu = C$  from a freshly scraped sample and an oxidized one.

#### ACKNOWLEDGMENTS

We acknowledge the French Synchrotron facility SOLEIL (Saint-Aubin, France) for the allocated beam time (exp. N° 20210307 and N° 20220725). A.C. thanks the National Science and Technology Council (NSTC) of the Republic of China, Taiwan, for financially supporting this research under Contract No. NSTC 111-2112-M-213-031.

#### APPENDIX A: OXIDATION EFFECT

Figure 5 shows a comparison between Ce  $M_5$ -edge XAS taken from a freshly scraped sample surface, and eight hours after scraping. The clean surface of the sample was prepared *in situ* by repeatedly scraping with a diamond file under the base pressure of  $1 \times 10^{-8}$  mbar. We have checked the sample cleanliness by the absence of the  $\text{CeO}_2$  contribution in the spectra. The Ce  $M_5$ -edge XAS profile line shape of the oxidized surface is significantly changed compared to the clean one. Typically, a shoulder and a satellite structure arise, respectively, at 884 eV and 890 eV (indicated by arrows A and C, respectively). The spectrum is the sum of two contributions associated, respectively, to  $\text{Ce}_{0.93}\text{Sc}_{0.07}$  alloy in the bulk and to the oxidized surface ( $\text{CeO}_2$ ). Satellite B remains at the same

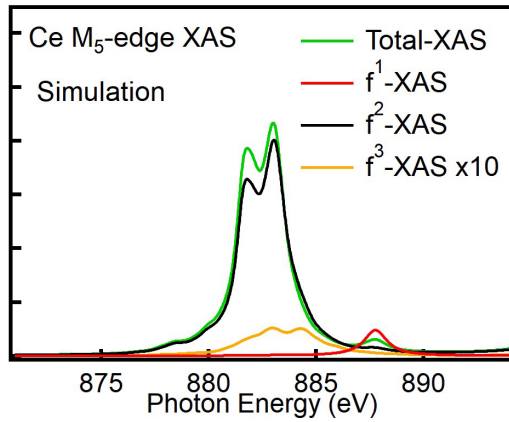


FIG. 7. Calculated XAS spectra at Ce-M5 edge and the contribution associated with the different configurations ( $d^{10}f^0 \rightarrow d^9f^1$ ,  $d^{10}f^1L \rightarrow d^9f^2L$  and  $d^{10}f^2L^2 \rightarrow d^9f^3L^2$ ). It should be noted that the total XAS is not the sum of  $f^1$ ,  $f^2$ , and  $f^3$  contributions due to interference effects.

energy but gets masked by the surface contribution. Indeed, shoulder A and satellite C are, respectively, associated with the  $3d^94f^2$  and  $3d^94f^1$  final states of the oxidized surface corresponding to  $\text{CeO}_2$  [38].

The Ce  $M_5$ -edge RIXS spectra taken at the incident photon energies  $h\nu = B$  and  $h\nu = C$  from the clean and oxidized surface are, respectively, shown in Figs. 6(a) and 6(b). Interestingly, the RIXS spectral line shape is unaffected by the oxidation effects when the incident photon energy is tuned at  $h\nu = B$  (the bulk satellite), while this satellite is almost invisible in the XAS spectra of the oxidized surface. However, when the incident photon energy is tuned at  $h\nu = C$  (the surface satellite), a prominent structure arises at about 6.5 eV of the RIXS spectrum measured for the oxidized surface. These two behaviors highlight two characteristics of RIXS: its bulk sensitivity and its chemical sensitivity. Especially, tuning the incoming photon energy on different features of the same edge allows for prioritizing the scattering from a given element in the studied material. Here, the  $\text{Ce}_{0.93}\text{Sc}_{0.07}$  in the bulk, or the  $\text{CeO}_2$  of the oxidized surface.

## APPENDIX B: FULL MULTIPLY CONFIGURATION INTERACTION CALCULATIONS

The XAS and RIXS spectra were simulated using a simplified version (the zero bandwidth limit) of the Gunnarsson and Schönhammer model [63], combined with full-multiplet calculations [50,51]. The simulations were performed with the QUANTY code [53,54] and the Slater integrals for the  $4f$ - $4f$  and  $3d$ - $4f$  electron-electron interactions were taken from

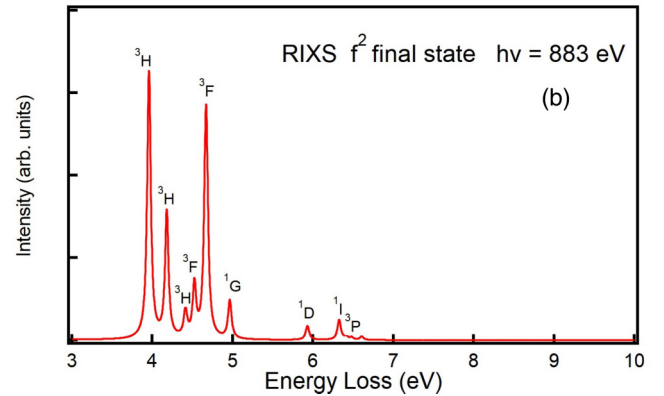
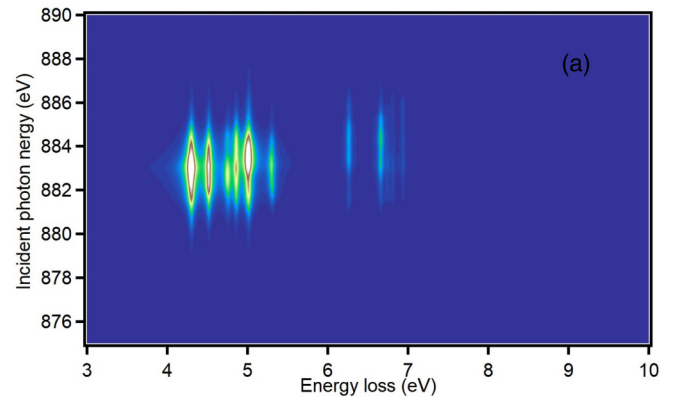


FIG. 8. (a) RIXS map in the energy loss range of the  $f^2$  final state. (b) RIXS spectra at  $h\nu = 883$  eV.

the Crispy [64] implementation of the Quany code. A reduction factor of 80% of the Hartree-Fock values of the Slater integrals has been used to consider the screening of the intraatomic electron-electron interactions by the presence of other charges. Three configurations have been used, namely  $f^0$ ,  $f^1L$ , and  $f^2L^2$  for the initial state of RIXS and  $d^9f^1$ ,  $d^9f^2L$ , and  $d^9f^3L^2$  for the intermediate state of RIXS (XAS final state). Using the parameters given in Table I, we calculated the XAS and RIXS spectra of  $\text{Ce}_{0.93}\text{Sc}_{0.07}$  in the  $\gamma$  and  $\alpha$  phases, as shown in Figs. 1, 3(c), and 3(d).

Taking into account the  $d^9f^3L^2$  is crucial to reproduce the RIXS spectra, although its contribution is mainly hidden in the XAS spectra. In order to visualize its contribution in the XAS spectra, we have calculated the partial spectral weights from each configuration in the ground state (see Fig. 7). The RIXS map in the energy loss range of the  $f^2$  final state is shown in Fig. 8. A small Lorentzian broadening of 0.05 eV FWHM has been used in order to show the multiplet structures. For the incident photon energy tuned at 883 eV, the  $f^2$  final state is composed of the lower energy  $^3H$ ,  $^3F$ ,  $^1G$  multiplets and the higher energy  $^1D$ ,  $^1I$ ,  $^3P$  multiplet.

[1] A. C. Hewson, *The Kondo Problem to Heavy Fermions* (Cambridge University Press, Cambridge, 1993).

[2] P. Coleman, in *Handbook of Magnetism and Advanced Magnetic Materials*, edited by H. Kronmüller, S. Parkin, and I. Zutic (John Wiley and Sons, 2007), Vol. 1, pp. 95–148.

[3] N. E. Bickers, D. L. Cox, and J. W. Wilkins, *Phys. Rev. B* **36**, 2036 (1987); N. E. Bickers, *Rev. Mod. Phys.* **59**, 845 (1987) and references therein.

[4] D. C. Koskenmaki and K. A. Gschneidner, Jr., in *Metals*, edited by K. A. Gschneidner, Jr. and L. Eyring, Handbook on the



- Physics and Chemistry of Rare Earths Vol. 1 (Elsevier, New York, 1978), p. 337.
- [5] J.-P. Rueff, J.-P. Itié, M. Taguchi, C. F. Hague, J.-M. Mariot, R. Delaunay, J.-P. Kappler, and N. Jaouen, *Phys. Rev. Lett.* **96**, 237403 (2006).
- [6] C. Dallera, M. Grioni, A. Palenzona, M. Taguchi, E. Annese, G. Ghiringhelli, A. Tagliaferri, N. B. Brookes, Th. Neisius, and L. Braicovich, *Phys. Rev. B* **70**, 085112 (2004).
- [7] B. Chen, E. M. Pärshcke, W.-C. Chen, B. Scoggins, B. Li, M. Balasubramanian, S. Heald, J. Zhang, H. Deng, R. Sereika, Y. Sorb, X. Yin, Y. Bi, K. Jin, Q. Wu, C.-C. Chen, Y. Ding, and H.-K. Mao, *J. Phys. Chem. Lett.* **10**, 7890 (2019).
- [8] J.-P. Rueff, C. F. Hague, J.-M. Mariot, L. Journel, R. Delaunay, J.-P. Kappler, G. Schmerber, A. Derory, N. Jaouen, and G. Krill, *Phys. Rev. Lett.* **93**, 067402 (2004).
- [9] D. M. Wieliczka, C. G. Olson, and D. W. Lynch, *Phys. Rev. B* **29**, 3028 (1984).
- [10] F. Patthey, B. Delley, W. D. Schneider, and Y. Baer, *Phys. Rev. Lett.* **55**, 1518 (1985).
- [11] E. Weschke, C. Laubschat, T. Simmons, M. Domke, O. Strebel, and G. Kaindl, *Phys. Rev. B* **44**, 8304 (1991).
- [12] J. J. Joyce, A. J. Arko, J. Lawrence, P. C. Canfield, Z. Fisk, R. J. Bartlett, and J. D. Thompson, *Phys. Rev. Lett.* **68**, 236 (1992).
- [13] E. Weschke, A. Hohn, G. Kaindl, S. L. Molodtsov, S. Danzenbacher, M. Richter, and C. Laubschat, *Phys. Rev. B* **58**, 3682 (1998).
- [14] M. Higashiguchi, K. Shimada, T. Narimura, H. Namatame, and M. Taniguchi, *Phys. B Condens. Matter* **351**, 256 (2004).
- [15] D. Wieliczka, J. H. Weaver, D. W. Lynch, and C. G. Olson, *Phys. Rev. B* **26**, 7056 (1982).
- [16] Y. Baer and G. Busch, *Phys. Rev. Lett.* **31**, 35 (1973).
- [17] Y. Baer and G. Busch, *J. Electron Spectrosc. Relat. Phenom.* **5**, 611 (1974).
- [18] E. Wuilloud, H. R. Moser, W. -D. Schneider, and Y. Baer, *Phys. Rev. B* **28**, 7354 (1983).
- [19] M. Grioni, P. Weibel, D. Malterre, Y. Baer, and L. Du'o, *Phys. Rev. B* **55**, 2056 (1997).
- [20] L. J. P. Ament, M. van Veenendaal, T. P. Devereaux, J. P. Hill and J. van den Brink, *Rev. Mod. Phys.* **83**, 705 (2011).
- [21] A. Kotani and S. Shin, *Rev. Mod. Phys.* **73**, 203 (2001).
- [22] Yu. Kucherenko, S. L. Molodtsov, M. Heber, and C. Laubschat, *Phys. Rev. B* **66**, 155116 (2002).
- [23] L. Z. Liu, J. W. Allen, O. Gunnarsson, and N. E. Christensen, and O. K. Andersen, *Phys. Rev. B* **45**, 8934 (1992).
- [24] T. Uozumi, K. Kanai, S. Shin, A. Kotani, G. Schmerber, J. P. Kappler, and J. C. Parlebas, *Phys. Rev. B* **65**, 045105 (2002).
- [25] S. M. Butorin, D. C. Mancini, J.-H. Guo, N. Wassdahl, J. Nordgren, M. Nakazawa, S. Tanaka, T. Uozumi, A. Kotani, Y. Ma, K. E. Myano, B. A. Karlin, and D. K. Shuh, *Phys. Rev. Lett.* **77**, 574 (1996).
- [26] S. M. Butorin, M. Magnuson, K. Ivanov, D. K. Shuh, T. Takahashi, S. Kunii, J.-H. Guo, and J. Nordgren, *J. Electron Spectrosc. Relat. Phenom.* **101-103**, 783 (1999).
- [27] M. Nakazawa, S. Tanaka, T. Uozumi, and A. Kotani, *J. Phys. Soc. Jpn.* **65**, 2303 (1996).
- [28] M. Magnuson, S. M. Butorin, J.-H. Guo, A. Agui, J. Nordgren, H. Ogasawara, A. Kotani, T. Takahashi, and S. Kunii, *Phys. Rev. B* **63**, 075101 (2001).
- [29] A. Amorese, G. Dellea, M. Fanciulli, S. Seiro, C. Geibel, C. Krellner, I. P. Makarova, L. Braicovich, G. Ghiringhelli, D. V. Vyalikh, N. B. Brookes, and K. Kummer, *Phys. Rev. B* **93**, 165134 (2016).
- [30] A. Amorese, N. Caroca-Canales, S. Seiro, C. Krellner, G. Ghiringhelli, N. B. Brookes, D. V. Vyalikh, C. Geibel, and K. Kummer, *Phys. Rev. B* **97**, 245130 (2018).
- [31] A. Amorese, K. Kummer, N. B. Brookes, O. Stockert, D. T. Adroja, A. M. Strydom, A. Sidorenko, H. Winkler, D. A. Zocco, A. Prokofiev, S. Paschen, M. W. Haverkort, L. H. Tjeng, and A. Severing, *Phys. Rev. B* **98**, 081116(R) (2018).
- [32] A. Amorese, D. Khalyavin, K. Kummer, N. B. Brookes, C. Ritter, O. Zaharko, C. B. Larsen, O. Pavlosiuk, A. P. Pikul, D. Kaczorowski, M. Gutmann, A. T. Boothroyd, A. Severing, and D. T. Adroja, *Phys. Rev. B* **105**, 125119 (2022).
- [33] A. Amorese, P. Hansmann, A. Marino, P. Körner, T. Willers, A. Walters, K.-J. Zhou, K. Kummer, N. B. Brookes, H.-J. Lin, C.-T. Chen, P. Lejay, M. W. Haverkort, L. H. Tjeng, and A. Severing, *Phys. Rev. B* **107**, 115164 (2023).
- [34] G. Zhao, H. Li, W. Lin, Q. Ren, J. Denlinger, Y.-D. Chuang, X. Zhang, L. A. Wray, and L. Miao, *Phys. Rev. B* **107**, 245149 (2023).
- [35] A. Kotani, *Phys. Rev. B* **83**, 165126 (2011).
- [36] J. N. Hancock, M. Dzero, J. Sarrao, T. Schmitt, V. Strocov, M. Guarise, M. Grioni, *Phys. Rev. B* **98**, 075158 (2018).
- [37] M. C. Rahn, K. Kummer, A. Hariki *et al.* *Nat. Commun.* **13**, 6129 (2022).
- [38] M. Watanabe, Y. Harada, M. Nakazawa, Y. Ishiwata, R. Euguchi, T. Takeuchi, A. Kotani, and S. Shin, *Surf. Rev. Lett.* **09**, 983 (2002).
- [39] S. M. Butorin, D. C. Mancini, J.-H. Guo, N. Wassdahl, and J. Nordgren, *J. Alloys Compd.* **225**, 230 (1995).
- [40] B. T. Chiego, J. Okamoto, J.-H. Li, T. Ohkochi, H.-Y. Huang, D.-J. Huang, C.-T. Chen, C.-N. Kuo, C.-S. Lue, A. Chainani, and D. Malterre, *Phys. Rev. B* **106**, 075141 (2022).
- [41] K.-J. Zhou, M. Radovic, J. Schlappa, V. Strocov, R. Frison, J. Mesot, L. Patthey, and T. Schmitt, *Phys. Rev. B* **83**, 201402(R) (2011).
- [42] F. Pfaff, H. Fujiwara, G. Berner, A. Yamasaki, H. Niwa, H. Kiuchi, A. Gloskovskii, W. Drube, J. Gabel, O. Kirilmaz, A. Sekiyama, J. Miyawaki, Y. Harada, S. Suga, M. Sing, and R. Claessen, *Phys. Rev. B* **97**, 035110 (2018).
- [43] T. Schmitt, L.-C. Duda, M. Matsubara, M. Mattesini, M. Klemm, A. Augustsson, J.-H. Guo, T. Uozumi, S. Horn, R. Ahuja, A. Kotani, and J. Nordgren, *Phys. Rev. B* **69**, 125103 (2004).
- [44] V. Bisogni, S. Catalano, R. J. Green, M. Gibert, R. Scherwitzl, Y. Huang, V. N. Strocov, P. Zubko, S. Balandeh, J.-M. Triscone, G. Sawatzky, and T. Schmitt, *Nat. Commun.* **7**, 13017 (2016).
- [45] A. Hariki, M. Winder, and J. Kuneš, *Phys. Rev. Lett.* **121**, 126403 (2018).
- [46] S. G. Chiuzbâian, C. F. Hague, A. Avila, R. Delaunay, N. Jaouen, M. Sacchi, F. Polack, M. Thomasset, B. Lagarde, A. Nicolaou, S. Brignolo, C. Baumier, J. Lüning, and J.-M. Mariot, *Rev. Sci. Instrum.* **85**, 043108 (2014).
- [47] M. Sacchi, N. Jaouen, H. Popescu, R. Gaudemer, J. M. Tonnerre, S. G. Chiuzbâian, C. F. Hague, A. Delmotte, J. M. Dubuisson, G. Cauchon, B. Lagarde, and F. Polack, *J. Phys.: Conf. Ser.* **425**, 072018 (2013).



- [48] J. C. Fuggle, F. U. Hillebrecht, Z. Zolnierrek, R. Lässer, C. Freiburg, O. Gunnarsson, and K. Schönhammer, *Phys. Rev. B* **27**, 7330 (1983).
- [49] T. Willers, D. T. Adroja, B. D. Rainford, Z. Hu, N. Hollmann, P. O. Körner, Y.-Y. Chin, D. Schmitz, H. H. Hsieh, H.-J. Lin, C. T. Chen, E. D. Bauer, J. L. Sarrao, K. J. McClellan, D. Byler, C. Geibel, F. Steglich, H. Aoki, P. Lejay, A. Tanaka *et al.* *Phys. Rev. B* **85**, 035117 (2012).
- [50] J. M. Imer and E. Wuilloud, *Z. Phys. B* **66**, 153 (1987).
- [51] M. Sundermann, F. Strigari, T. Willers, J. Weinen, Y. F. Liao, K.-D. Tsuei, N. Hiraoka, H. Ishii, H. Yamaoka, J. Mizuki, Y. Zekko, E. D. Bauer, J. L. Sarrao, J. D. Thompson, P. Lejay, Y. Muro, K. Yutani, T. Takabatake, A. Tanaka, N. Hollmann *et al.* *J. Electron Spectrosc. Relat. Phenom.* **209**, 1 (2016).
- [52] C. W. Chuang, B. Tegomo Chiogo, D. Malterre, P.-Y. Chuang, C.-M. Cheng, T.-W. Pi, F.-H. Chang, H.-J. Lin, C.-T. Chen, C.-N. Kuo, C.-S. Lue and A. Chainani, *Electron. Struct.* **3**, 034001 (2021).
- [53] M. W. Haverkort, M. Zwierzycki, and O. K. Andersen, *Phys. Rev. B* **85**, 165113 (2012).
- [54] M. W. Haverkort, *J. Phys.: Conf. Ser.* **712**, 012001 (2016).
- [55] K. Kanai, Y. Tezuka, T. Terashima, Y. Muro, M. Ishikawa, T. Uozumi, A. Kotani, G. Schmerber, J. P. Kappler, J. C. Parlebas, and S. Shin, *Phys. Rev. B* **60**, 5244 (1999).
- [56] M. Nakazawa, H. Ogasawara, and A. Kotani, *J. Phys. Soc. Jpn.* **69**, 4071 (2000).
- [57] N. Sasabe, H. Tonai, and T. Uozumi, *J. Phys. Soc. Jpn.* **86**, 093701 (2017).
- [58] M. Nakazawa and A. Kotani, *J. Phys. Soc. Jpn.* **71**, 2804 (2002).
- [59] N. Sasabe and T. Uozumi, *J. Phys. Soc. Jpn.* **92**, 054706 (2023).
- [60] S. Banik, A. Arya, A. Bendounan, M. Maniraj, A. Thamizhavel, I. Vobornik, S. K. Dhar, S. K. Deb, *J. Phys.: Condens. Matter* **26**, 335502 (2014).
- [61] J. K. Lang, Y. Baer, and P. A. Cox, *Phys. Rev. Lett.* **42**, 74 (1979).
- [62] K. A. Gschneider, R. O. Elliott, and R. R. McDonald, *J. Phys. Chem. Solids* **23**, 1191 (1962).
- [63] O. Gunnarsson and K. Schönhammer, *Phys. Rev. B* **28**, 4315 (1983).
- [64] M. Retegan, Crispy: v0.7.3 (2019), doi:10.5281/zenodo.1008184.